Ultrawide Bandgap Vertical β-$(Al_xGa_{1-x})_2O_3$ Schottky Barrier Diodes on Free-Standing β-Ga_2O_3 Substrates

Dinusha Herath Mudiyanselage, Dawei Wang, and Houqiang Fu*.

School of Electrical, Computer, and Energy Engineering, Arizona State University, Tempe, AZ 85287, USA

**Email: houqiang@asu.edu*

Abstract— Ultrawide bandgap β-$(Al_xGa_{1-x})_2O_3$ vertical Schottky barrier diodes (SBDs) on (010) β-Ga_2O_3 substrates are demonstrated. The β-$(Al_xGa_{1-x})_2O_3$ epilayer has an Al composition of 21% and a nominal Si doping of 2×10^{17} cm^{-3} grown by molecular beam epitaxy. Pt/Ti/Au has been employed as the top Schottky contact, whereas Ti/Au has been utilized as the bottom Ohmic contact. The fabricated devices show excellent rectification with a high on/off ratio of ~10^9, a turn-on voltage of 1.5 V, and an on-resistance of 3.4 mΩ.cm^2. Temperature-dependent forward current-voltage characteristics show effective Schottky barrier height varied from 0.91 to 1.18 eV while the ideality factor from 1.8 to 1.1 with increasing temperatures, which is ascribed to the inhomogeneity of the metal/semiconductor interface. The Schottky barrier height was considered as a Gaussian distribution of potential, where the extracted mean barrier height and a standard deviation at zero bias were 1.81 eV and 0.18 eV, respectively. A comprehensive analysis of the device leakage was performed to identify possible leakage mechanisms by studying temperature-dependent reverse current-voltage characteristics. At reverse bias, due to the large Schottky barrier height, the contributions from thermionic emission and thermionic field emission are negligible. By fitting reverse leakage currents at different temperatures, it was identified that Poole-Frenkel emission and trap-assisted tunneling are the main leakage mechanisms at high and low temperature regimes, respectively. Electrons can tunnel through the Schottky barrier assisted by traps at low temperatures, while they can escape these traps at high temperatures and be transported under high electric fields. This work can serve as an important reference for the future development of

ultrawide bandgap β-$(Al_xGa_{1-x})_2O_3$ power electronics, RF electronics, and ultraviolet (UV) photonics.

Keywords— β-$(Al_xGa_{1-x})_2O_3$, Schottky barrier diodes, vertical device, reverse leakage analysis

I. INTRODUCTION

Ultrawide bandgap (UWBG) semiconductors have garnered considerable attention in recent years due to their promising applications in power electronics, optoelectronics, and RF electronics[1-8]. β-Ga_2O_3 is a promising candidate for UWBG semiconductors due to a high breakdown field of 8 MV/cm and a large bandgap of 4.6-4.9 eV, and a high Baliga's Figure of Merit (BFOM) compared with GaN and SiC[9]. Furthermore, due to the availability of large native substrates, β-Ga_2O_3 has great potential for cost-effective high-voltage power electronics[10]. Moreover, alloying Ga_2O_3 with Al_2O_3 can produce $(Al_xGa_{1-x})_2O_3$ with increased bandgap (e.g., 4.8-6.2 eV for x = 0 to 0.71)[11]. β-$(Al_xGa_{1-x})_2O_3$ is a monoclinic ternary alloy that is expected to have a higher BFOM than Ga_2O_3, making it more suitable for power electronic applications[3]. Recently, there have been several optoelectronic and power devices demonstrated using β-$(Al_xGa_{1-x})_2O_3$. Chen *et al.*[12] reported the effect of O_2 concentration on sputtered $(Al_xGa_{1-x})_2O_3$ films for deep UV photodetectors. β-$(Al_xGa_{1-x})_2O_3/Ga_2O_3$ heterojunction modulation-doped field effect transistors (MODFETs) have been extensively studied[13-19]. Zhang *et al.*[15] reported record low-temperature mobility of ~2700 cm^2/Vs in β-$(Al_xGa_{1-x})_2O_3/Ga_2O_3$ heterostructure. Furthermore, Okumura *et al.*[13] demonstrated β-$(Al_xGa_{1-x})_2O_3$ metal-semiconductor field effect transistors (MESFETs). However, most of these power devices are lateral devices where the currents flow laterally, and voltages are handled laterally. These lateral devices usually underperform compared

with their material limits. In commercial Si and SiC power devices, vertical architecture dominates, especially for high-voltage high-power applications, due to larger current and voltage handling capability, avalanche capability, no surface-related issues, better heat dissipation, and smaller chip area.

To date, there are very few reports of vertical β-$(Al_xGa_{1-x})_2O_3$ devices. One of the major challenges is growing high-quality β-$(Al_xGa_{1-x})_2O_3$ layers with high Al contents (e.g., >20% on (010) β-Ga_2O_3 substrates)[13]. This is because β-Ga_2O_3 crystallizes in a monoclinic structure, and Al_2O_3 prefers a conundrum structure, leading to phase separation at high Al contents[20]. Furthermore, due to the lattice mismatch with sufficiently high Al composition, epitaxial growth of β-$(Al_xGa_{1-x})_2O_3$ on β-Ga_2O_3 is challenging. Moreover, Schottky and ohmic contact behavior on β-$(Al_xGa_{1-x})_2O_3$ needs to be further understood comprehensively. However, ohmic and Schottky contact behavior on β-Ga_2O_3 is extensively investigated in the past few years[21,22]. Jadhav *et al.*[23] investigated temperature dependent barrier height inhomogeneity in β-Ga_2O_3 Schottky barrier diodes. Ahmadi *et al.*[20] found Schottky barrier heights of Ni to β-$(Al_xGa_{1-x})_2O_3$ with different Al compositions, which was attributed to the lateral fluctuation of Al alloy composition. Furthermore, β-$(Al_xGa_{1-x})_2O_3$ power devices suffer from low breakdown voltages and high leakage current. A systematic investigation of the leakage mechanism and the temperature-dependent characteristics of β-$(Al_xGa_{1-x})_2O_3$ devices are still lacking. In this work, we demonstrate vertical β-$(Al_xGa_{1-x})_2O_3$ (x = 0.21) Schottky barrier diodes (SBDs) on free-standing (edge-defined film-fed grown) highly doped (010) β-Ga_2O_3 substrates and systematically investigate their temperature-dependent forward and reverse electrical characteristics. Different models have been used to comprehensively understand the leakage mechanisms of the vertical β-$(Al_xGa_{1-x})_2O_3$ SBDs. This work can serve as

an important reference for the design of high-voltage high power vertical β-$Al_x(Ga_{1-x})_2O_3$ power devices.

II. EXPERIMENTAL

200 nm β-$(Al_xGa_{1-x})_2O_3$ (x = 0.21) layer was grown using molecular beam epitaxy (MBE) on edge-defined film-fed grown (010) β-Ga_2O_3 substrate [Fig. 1] by Novel Crystal Technology, Inc, Japan. During the MBE growth, Ga and Al are evaporated from effusion cells in RF-generated oxygen plasma to form β-$(Al_xGa_{1-x})_2O_3$ thin films[24,25]. The Al composition of the grown film can be estimated by the shift of β-Ga_2O_3 and β-$(Al_xGa_{1-x})_2O_3$ (020) peak from the XRD spectra[26]. More details about the MBE growth and Al content determination can be found elsewhere[24,25,26]. The β-Ga_2O_3 substrate is heavily doped with [Sn] = 3.1×10^{18} cm^{-3}, while Si doping concentration in β-$(Al_xGa_{1-x})_2O_3$ layer was estimated to be 2.0×10^{17} cm^{-3}. Atomic force microscopy (AFM) suggested a film surface RMS roughness of 2.6 nm [Fig. 1(d)], and X-ray diffraction (XRD) confirmed the (020) β-$(Al_xGa_{1-x})_2O_3$ peak [Fig. 1(b)] of the film. The device fabrication started with sample cleaning using acetone, isopropyl alcohol (IPA), and distilled water. Then a 200 nm Ni hard mask was deposited by electron beam (E-beam) evaporation on the film using standard photolithography and liftoff. This Ni hard mask protects the etching of β-$(Al_xGa_{1-x})_2O_3$ during mesa isolation of the devices. Next, SF_6 inductive-coupled plasma reactive ion etching (ICP-RIE) was performed at 400 W until a mesa depth of 300 nm was obtained. The Ni hard mask was removed using a Ni etchant, followed by sample cleaning using HF and H_2SO_4 to remove the etching damage induced by the ICP-RIE dry etching. Then Ti/Au (20/130) nm cathode (Ohmic contact) was deposited at the back side of the β-Ga_2O_3 substrate using E-beam evaporation

followed by 500 °C rapid thermal annealing (RTA) in N_2 environment. Finally, Pt/Ti/Au (20/10/120) nm anode (Schottky Contact) was deposited by E-beam evaporation and formed using standard photolithography and liftoff. Figure 1(a) shows the schematic of the fabricated vertical β-$(Al_xGa_{1-x})_2O_3$ SBDs on β-Ga_2O_3 substrate. The diameter of the SBD (ϕ) is 100 µm. Current density-voltage (*J-V*) measurements of the fabricated devices were measured using a probe station with a hotplate and a Keithley 2470 source meter. Capacitance-Voltage (*C-V*) measurements were performed on a Hewlett-Packard 4275A LCR meter.

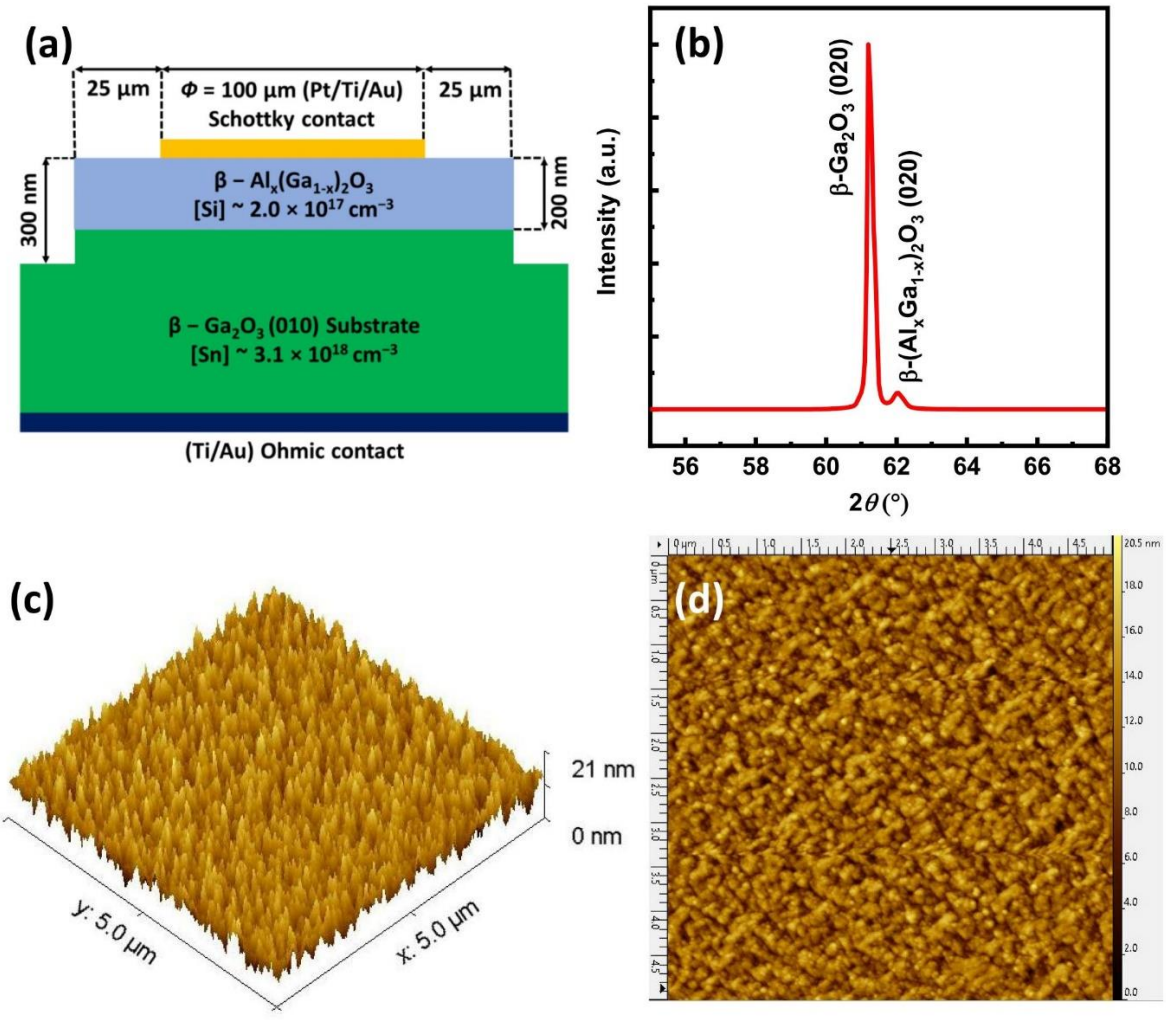

Figure 1. (a) Schematic of fabricated vertical β-$(Al_xGa_{1-x})_2O_3$ (x = 0.21) SBD. (b) XRD spectrum of (020) peaks of β-Ga_2O_3 and β-$(Al_xGa_{1-x})_2O_3$. (c) 3D AFM data of the epilayer. (d) Top view of the epilayer by AFM.

III. RESULTS AND DISCUSSION

Fig. 2(a)-(b) shows the forward characteristics of the vertical β-$(Al_xGa_{1-x})_2O_3$ SBD at room temperature. The device exhibited a turn-on voltage of ~1.5 V, a specific on-resistance of 3.4 mΩ.cm^2 at +5 V, and an on/off ratio of ~10^9. The *C-V* measurements were performed at room temperature using 1 MHz frequency. Fig. 2(c) indicates a carrier concentration of 2.8 × 10^{17} cm^{-3} in the β-$(Al_xGa_{1-x})_2O_3$ film, which is close to the nominal Si doping. The temperature-dependent forward *J-V* characteristics of the device are presented in Fig. 2(d). The measured electrical characteristics are quite stable and reproducible among many devices across the wafer. The devices after high-temperature testing retain the initial *J-V* curves even after cooling down to room temperature. Using the diode thermionic emission (TE) model, Schottky barrier height (φ_b) and ideality factor (n) of the vertical β-$Al_x(Ga_{1-x})_2O_3$ SBD can be calculated. For $V > 3kT$, the TE model can be expressed as[27]

$$J = J_s\left[\exp\left(\frac{qV}{nkT}\right) - 1\right] \qquad (1)$$

$$J_s = A^*T^2 \exp\left(-\frac{q\varphi_{eff}}{kT}\right) \qquad (2)$$

$$A^* = \frac{4\pi q k^2 m^*}{h^3} \qquad (3)$$

where J is the current density, J_s is the saturation current density, A^* is the Richardson constant, T is the temperature in kelvin, q is the electron charge, φ_{eff} is the effective Schottky barrier height,

n is the ideality factor, k is the Boltzmann constant, m^* is the effective electron mass, and h is the Planck constant.

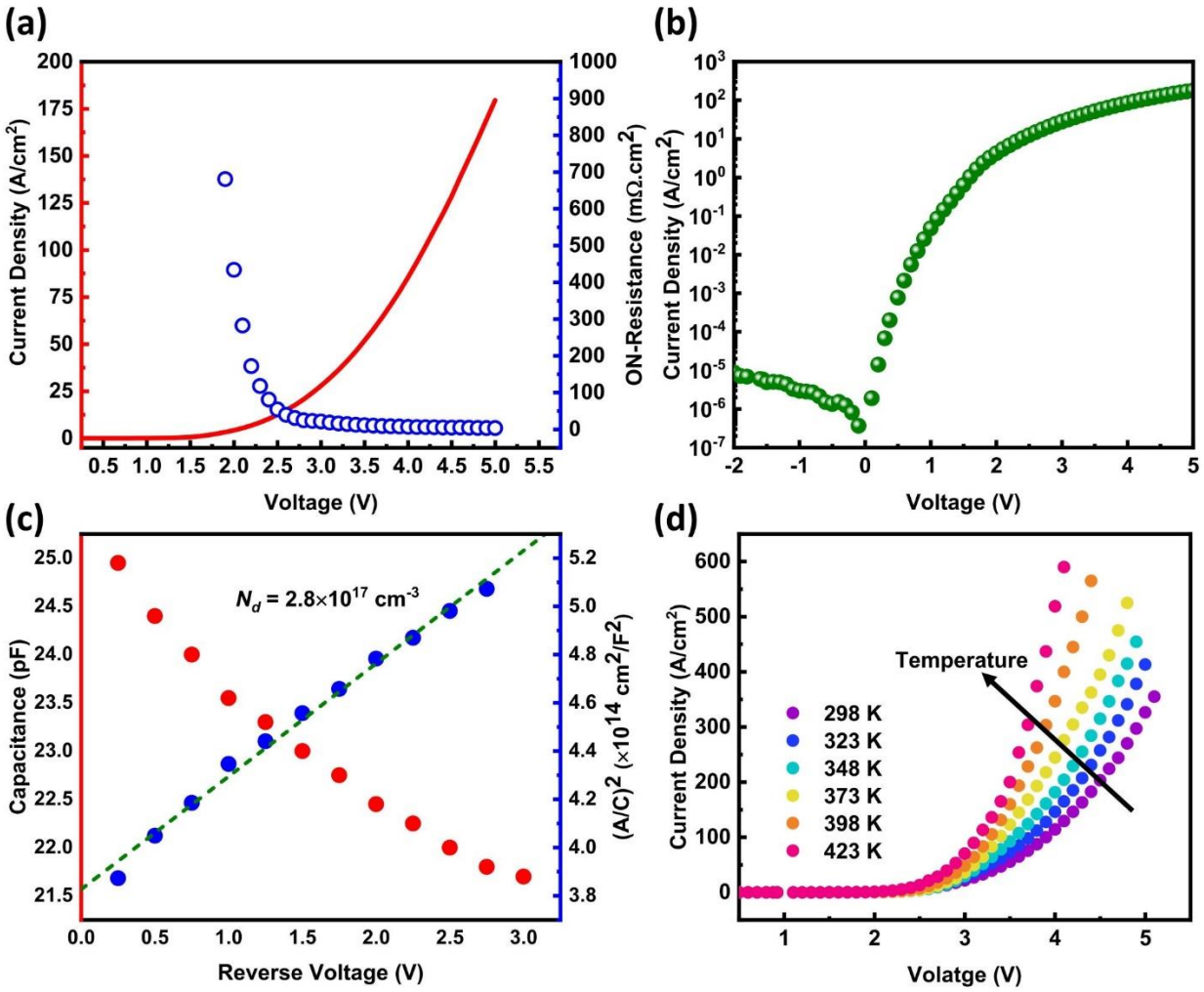

Figure 2. (a) Forward current density and specific R_{ON} as a function of voltage for the vertical β-$(Al_xGa_{1-x})_2O_3$ SBD. (b) Forward current density versus voltage for the vertical β-$(Al_xGa_{1-x})_2O_3$ SBD on a semi-log scale. (c) *C-V* and *1/C²-V* plots and (d) temperature-dependent *J-V* curves of the vertical β-$(Al_xGa_{1-x})_2O_3$ SBD.

Figure 3 shows the Schottky barrier heights and ideality factors of the vertical β-$(Al_xGa_{1-x})_2O_3$ SBD calculated using the TE model. It should be noted that the Richardson constant of 37.8 A/cm²K² was calculated using the reported effective electron mass of $0.313m_0$[3] for β-$(Al_xGa_{1-}$

$_x$)$_2$O$_3$. With increasing temperature, φ_{eff} varied from 0.91 to 1.18 eV, while the n changed from 1.8 to 1.1 [Fig. 3(a)]. There is a clear temperature dependence of both parameters, which stem from the inhomogeneous metal/semiconductor interface[28,29]. In Fig. 3(b), a linear correlation between φ_{eff} and n was observed, which is a well-known phenomenon in the presence of an inhomogeneous Schottky contact. In the metal/semiconductor interface, there are regions with low and high Schottky barrier heights. At low temperatures, electrons can only pass through low Schottky barrier height regions, whereas at high temperatures, electrons gain momentum to cross high Schottky barrier height regions. As a result, the Schottky barrier height increased with temperature. To further investigate this behavior, Schottky barrier height can be considered as a Gaussian distribution of potential with a mean barrier height $\overline{\varphi_b}$ and a standard deviation σ, and the barrier is linearly dependent on voltage as follows:

$$\varphi_{eff} = \overline{\varphi_b} - \frac{q\sigma^2}{2kT} \qquad (4)$$

$$\overline{\varphi_b} = \overline{\varphi_{b0}} + \gamma V \qquad (5)$$

$$\sigma^2 = {\sigma_0}^2 - \xi V \qquad (6)$$

where φ_{b0} and σ_0 are the values at zero bias, and the coefficients γ and ξ represent the voltage-induced deformation of the Schottky barrier distribution[30]. Substituting Eq. (5) and (6) into Eq. (4) and combining Eq. (1) and (2), the ideality factor can be written as[31,32,33]

$$n^{-1} - 1 = -\gamma - \frac{q\xi}{2kT} \quad (7)$$

Therefore, Eq. (7) implies ideality factor becomes temperature-dependent, and its value can exceed unity. The voltage dependence of the Schottky barrier height and ideality factor was attributed to the interfacial states at the metal/semiconductor interface. These states become more negative with

applied forward bias, leading to an increase in the Schottky barrier height with bias and ideality factor greater than unity[32]. This voltage dependency of the Schottky barrier height can be interpreted as image force shifting the Schottky barrier maxima away from the metal-semiconductor into the semiconductor as the forward bias increases[33]. Furthermore, theoretical derivations suggest that both φ_{eff} and $(n^{-1}-1)$ are linear functions of inverse temperature $(1/T)$, which is in good agreement with the experimental results in Fig. 3(c) and (d). The extracted $\overline{\varphi_{b0}}$ and σ_0 were 1.81 eV and 0.18 eV, respectively. It is reported that Pt on (010) β-Ga_2O_3 has an ideal Schottky barrier height of up to 1.93 eV[34]. This work shows the mean Schottky barrier height at zero bias is 1.81 ± 0.18 eV, which is consistent with the ideal value.

It should be note that the *C-V* measurements did not correctly estimate the barrier height from Fig. 2(c). This discrepancy is likely due to two reasons. First, there is a frequency dispersion in the *C-V* measurements in WBG semiconductors. Due to this, the frequency which uses for the *C-V* measurements may not be the ideal frequency to measure the barrier height. At a particular frequency, some impurity states or donor states respond slowly to the applied AC electric field. To study this effect the, frequency dispersion *C-V* needs to be measured, which is out of the scope of this study. Second, the interfacial states between the metal and the semiconductor are insensitive to *C-V* measurements at low voltages. The inhomogeneity at the metal/semiconductor interface lowers the accuracy of the *C-V* measurements, which increases the uncertainty of the measured barrier height. However, barrier height measured from the *J-V* measurements are quite reliable as it represents the current flowing though the inhomogeneous Schottky barrier.

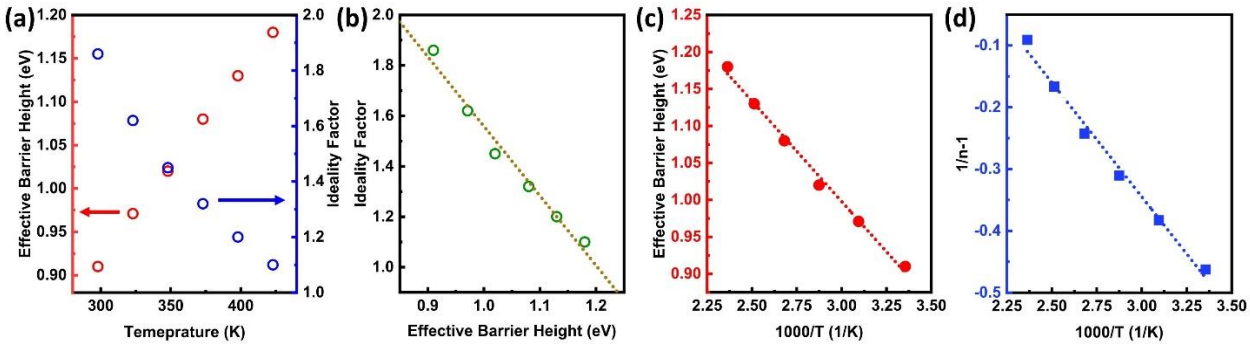

Figure 3. (a) Effective Schottky barrier height (φ_{eff}) and ideality factor (n) as a function of temperature for the vertical β-$(Al_xGa_{1-x})_2O_3$ SBD. (b) n versus φ_{eff}, (c) φ_{eff} versus 1000/T, and (d) $(\frac{1}{n}-1)$ versus 1000/T the vertical β-$(Al_xGa_{1-x})_2O_3$ SBD.

Figure 4(a) shows the temperature-dependent reverse *J-V* characteristics of the vertical β-$(Al_xGa_{1-x})_2O_3$ SBD. The reverse leakage current increased with increasing temperature. Figure 4(b) represents the current density as a function of 1/T at different reverse voltages. Different gradients in Fig. 4(b) corresponded to different leakage mechanisms. Figure 4(c) shows potential leakage mechanisms for SBDs. Different temperature regimes activate different processes inside the semiconductor, which can be investigated from the reverse *J-V* measurements. Due to the high Schottky barrier height of > 1 eV in the vertical β-$(Al_xGa_{1-x})_2O_3$ SBD, thermionic emission (TE) or thermionic field emission (TFE) is unlikely to be a major contributor to the reverse leakage of the device. The possible candidates for the vertical β-$(Al_xGa_{1-x})_2O_3$ SBD include Poole-Frenkel emission (PFE), trap-assisted tunneling (TAT), Fowler-Nordheim tunneling (FNT), field emission (FE), and variable range hopping (VRH). More details about these processes can be found elsewhere[35-41]. To identify the dominant process, fitting the reverse leakage data using the mathematical expression of each model is widely used. It was found that two dominant mechanisms were PFE and TAT, while the other mechanisms played a minor role.

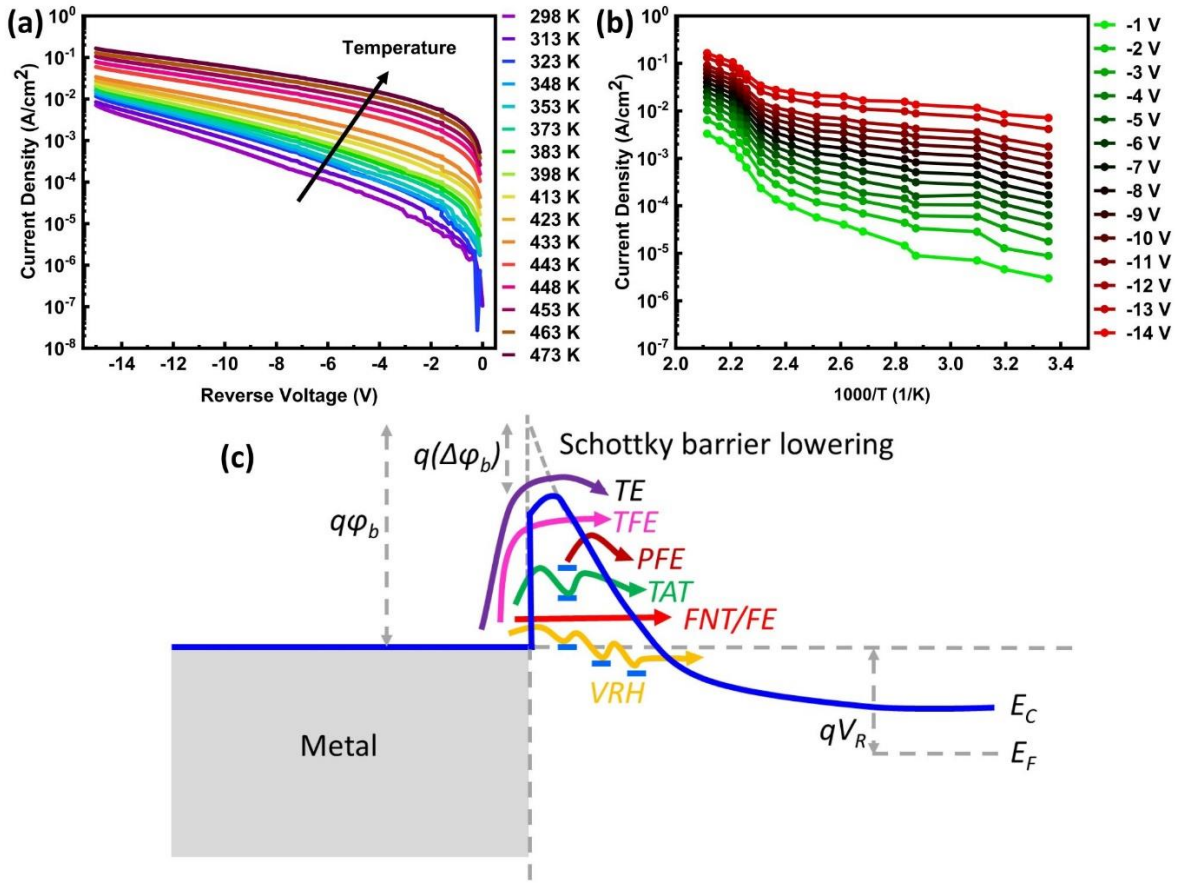

Figure 4. (a) Temperature-dependent reveres *J-V* characteristics of the vertical β-$(Al_xGa_{1-x})_2O_3$ SBD. (b) *J* versus 1000/*T* at different voltages for the vertical β-$(Al_xGa_{1-x})_2O_3$ SBD. (c) Potential leakage mechanisms in SBDs.

The PFE is a trap-mediated transport mechanism where the carrier density depends exponentially on the activation energy of the traps, and the current density due to PFE is given by[41]

$$J = CEexp\left[-\frac{q(\varphi_t - \sqrt{qE/\pi\varepsilon_0\varepsilon_s}}{kT}\right] \qquad (8)$$

where E is the electric field in the β-$(Al_xGa_{1-x})_2O_3$ layer, φ_t is the barrier height for electron emission from a trap state, ε_s is the high-frequency relative dielectric permittivity, ε_0 is the

permittivity of free space, C is a proportionality constant, and k is the Boltzmann's constant. It should be noted that the high-frequency (optical) dielectric constant, rather than the static one, should be used in the PFE equation[41]. Electrons can move slowly through an insulator or a semiconductor in the presence of a large electric field. Initially, electrons are in a localized or trap state and cannot move freely. With a high electric field, these localized electrons can be promoted to the conduction band and contribute to leakage currents. These electrons can move through the crystal before relaxing into another localized state. In other words, the PFE model describes an electric-field enhanced emission from a trap state which increases reverse leakage. From Eq. (8), $\ln\left(\frac{J}{E}\right)$ is a linear function of $\sqrt{E}$

$$\ln\left(\frac{J}{E}\right) = \frac{q}{kT}\sqrt{\frac{qE}{\pi\varepsilon_0\varepsilon_s}} - \frac{q\varphi_t}{kT} + \ln C = m(T)\sqrt{E} + b(T) \qquad (9)$$

Figure 5(a) indicates the PFE plot for the vertical β-$(Al_xGa_{1-x})_2O_3$ SBD between 373-473 K. Transport model based on the PFE in Eq. (9) shows a good agreement with the experimental data in this temperature regime with consistent Schottky barrier height and dielectric constant. Figure 5(b) shows the temperature-dependent slope $m(T)$ and intercept $b(T)$ extracted from Fig. 5(a). Both $m(T)$ and $b(T)$ are linear functions against inverse temperature, which is expected in the PFE model. The extracted dielectric constant ε_s and the emission barrier height φ_t for the device were $\varepsilon_s = 8.2$ and φ_t = 1.06 eV, which are consistent with experimental results[1,14,42]. The obtained φ_t is comparable with the extracted values from the TE model. These results indicate that the PFE mechanism is dominant at high temperatures (> 373 K).

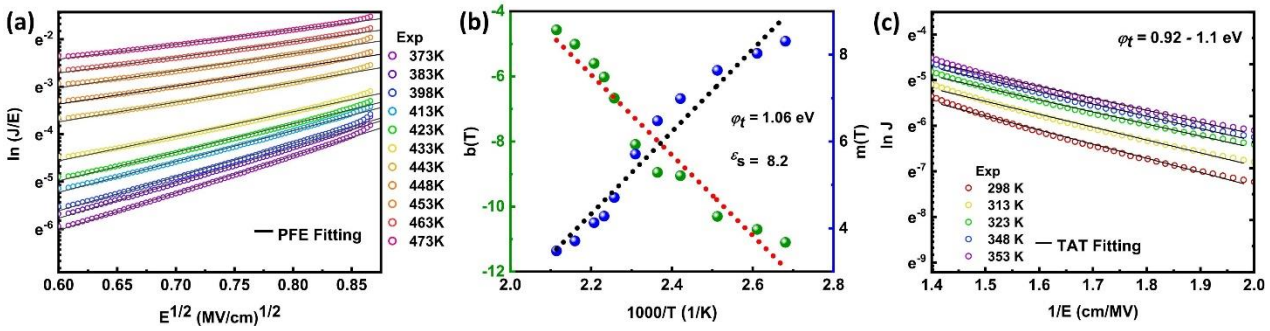

Figure 5. (a) Experimental and theoretical data of $\ln\left(\frac{J}{E}\right)$ versus $\sqrt{E}$ for the vertical β-$(Al_xGa_{1-x})_2O_3$ SBD. (b) The intercept $b(T)$ and the slope $m(T)$ of the curves in (a) are shown as a function of temperature. (c) Experimental and theoretical data of $\ln J$ versus $1/E$ at different temperatures.

Below 373 K, the leakage current of the vertical β-$(Al_xGa_{1-x})_2O_3$ SBD deviated from the PFE model and leaned towards the TAT model. In the TAT model, an electron in the metal could be activated to a trap state at the metal/semiconductor interface and then tunnel to the semiconductor side[43,44]. This model can be expressed by

$$J = Cexp\left[-\frac{4\sqrt{2qm^*}{\varphi_t}^{3/2}}{3\hbar E}\right] \qquad (10)$$

where φ_t is the barrier height for electron emission from a trap state, m^* is effective electron mass, C is a proportionality constant, and ħ is the reduced Planck's constant. The equation can be rearranged to find the φ_t from the measured reverse leakage current.

$$\ln(J) = -\frac{4\sqrt{2qm^*}{\varphi_t}^{3/2}}{3\hbar E} + lnC \qquad (11)$$

Figure 5(c) shows the measured and theoretical TAT plots for the vertical β-$(Al_xGa_{1-x})_2O_3$ SBD between 298-353 K. The extracted barrier height for electron emission from a trap state (φ_t) was between 0.92-1.1 eV. At low temperatures, electrons can tunnel through the Schottky barrier height

with the assistance of traps. With enough thermal energy at high temperatures, they can escape from the trap levels and transport under high electric fields (i.e., the PFE model). For high-voltage applications, growing thick β-$(Al_xGa_{1-x})_2O_3$ is needed and demands further research and development.

VI. CONCLUSION

We demonstrated vertical β-$(Al_xGa_{1-x})_2O_3$ SBDs on free-standing (010) β-Ga_2O_3 substrates. The device exhibited excellent forward rectifying behaviors with a high on/off ratio of ~10^9, a turn-on voltage of 1.5 V, and an on-resistance of 3.4 mΩ.cm^2. Temperature-dependence of the Schottky barrier height and ideality factor was due to the inhomogeneous metal/semiconductor interface. This interface inhomogeneity was explained by considering the Schottky barrier height as a Gaussian distribution with a mean Schottky barrier height of 1.81 eV at zero bias with a standard deviation of 0.18 eV. Comprehensive reverse leakage analysis indicated that PFE and TAT mechanisms were the main contributors to the reverse leakage currents of the device. The extracted physical parameters from the PFE and TAT models are consistent with experimental results. This work can serve as an important reference for future development of β-$(Al_xGa_{1-x})_2O_3$ based electronics and photonics for high-power, high-voltage, and ultraviolet (UV) photonic applications.

ACKNOWLEDGMENTS

Research supported as part of the ULTRA, an Energy Frontier Research Center funded by the U.S. Department of Energy (DOE), Office of Science, Basic Energy Sciences (BES), under Award # DE-SC0021230 (computational study) and by the National Science Foundation (NSF) under Award # 2302696 (experimental study and data analysis).

CONFLICT OF INTEREST

The authors have no conflicts to disclose.

DATA AVAILABILITY

The data that support the findings of this study are available from the corresponding author upon reasonable request.

REFERENCES

[1]S. J. Pearton, J. Yang, P. H. Cary IV, F. Ren, J. Kim, M. J. Tadjer, and M. A. Mastro, Appl. Phys. Rev. **5**, 011301 (2018).

[2]C. Wang, J. Zhang, S. Xu, C. Zhang, Q. Feng, Y. Zhang, J. Ning, S. Zhao, H. Zhou, and Y. Hao, J. Phys. D: Appl. Phys. **54**, 243001 (2021).

[3]A. Saikumar, S. Nehate, and K. Sundaram, Crit. Rev. Solid State Mater. Sci. **47**, (2021).

[4]N. Donato, N. Rouger, J. Pernot, G. Longobardi, and F. Udrea, J. Phys. D: Appl. Phys. **53**, 093001 (2020).

[5]R. Yu, G. Liu, G. Wang, C. Chen, M. Xu, H. Zhou, T. Wang, J. Yu, G. Zhao, and L. Zhang, J. Mat. Chem. C **9**, 1852 (2021).

[6]M. Higashiwaki, R. Kaplar, J. Pernot, and H. Zhao, Appl. Phys. Lett. **118**, 200401 (2021).

[7]H. Zhang, C. Huang, K. Song, H. Yu, C. Xing, D. Wang, Z. Liu, and H. Sun, Rep. Prog. Phys. **84** 044401 (2021).

[8]C. Huang, H. Zhang, H. Sun, Nano Energy **77** 105149 (2020).

[9]M. Higashiwaki and G. H. Jessen, Appl. Phys. Lett. **112**, 060401 (2018).

[10]H. Sun, K.-H. Li, C. G. T. Castanedo, S. Okur, G. S. Tompa, T. Salagaj, S. Lopatin, A. Genovese, and X. Li, Cryst. Growth Des. **18**, 2370 (2018)

[11]P. Ranga, A. Rishinaramangalam, J. Varley, A. Bhattacharyya, D. Feezell, and S. Krishnamoorthy, Appl. Phys. Express **12**, 111004 (2019).

[12]P. W. Chen, S. Y. Huang, C. C. Wang, S. H. Yuan, D. S. Wuu, J. Alloys Compd. 791 (2019).

[13]H. Okumura, Y. Kato, T. Oshima, and T. Palacios, Jpn. J. Appl. Phys. **58**, SBBD12 (2019).

[14]S. Krishnamoorthy, Z. Xia, C. Joishi, Y. Zhang, J. McGlone, J. Johnson, M. Brenner, A. R. Arehart, J. Hwang, S. Lodha, and S. Rajan, Appl. Phys. Lett. **111**, 023502 (2017).

[15]Y. Zhang, A. Neal, Z. Xia, C. Joishi, J. M. Johnson, Y. Zheng, S. Bajaj, M. Brenner, D. Dorsey, K. Chabak, G. Jessen, J. Hwang, S. Mou, J. P. Heremans, and S. Rajan, Appl. Phys. Lett. **112**, 173502 (2018)

[16]Y. Zhang, Z. Xia, J. McGlone, W. Sun, C. Joishi, A. R. Arehart, S. A. Ringel, and S. Rajan, IEEE Trans. Electron Devices **66**, 1574 (2019).

[17]E. Ahmadi, O. S. Koksaldi, X. Zheng, T. Mates, Y. Oshima, U. K. Mishra, and J. S. Speck, Appl. Phys. Express **10**, 071101 (2017).

[18]A. Vaidya, C. N. Saha, and U. Singisetti, IEEE Electron Device Lett. **42**, 1444 (2021).

[19]C. N. Saha, A. Vaidya, and U. Singisetti, Appl. Phys. Lett. **120**, 172102 (2022).

[20]E. Ahmadi, Y. Oshima, F. Wu, and J. S. Speck, Semicond. Sci. Technol. **32**, 035004 (2017).

[21]H. Sheoran, V. Kumar and R. Singh, ACS Appl. Electron. Mater. **4**, 2589 (2022).

[22]M.-H. Lee, R. L. Peterson, J. Mater. Res. **36**, 4771 (2021).

[23]A. Jadhav, L. A. M. Lyle, Z. Xu, K. K. Das, L. M. Porter, and B. Sarkar, J. Vac. Sci. Technol. B **39**, 040601 (2021).

[24]S. W. Kaun, F. Wu, and J. S. Speck, J. Vac. Sci. Technol. A **33**, 041508 (2015).

[25]T. Oshima, T. Okuno, N. Arai, Y. Kobayashi, and S. Fujita, Jpn. J. Appl. Phys. **48**, 070202 (2009).

[26]Y. Oshima, E. Ahmadi, S. C. Badescu, F. Wu, and J. S. Speck, Appl. Phys. Express **9**, 061102 (2016).

[27]S. M. Sze and K. K. Ng, Physics of Semiconductor Devices (Wiley, Hoboken, 2007).

[28]F. Iucolano, F. Roccaforte, F. Giannazzo, and V. Raineri, J. Appl. Phys. **102**, 113701 (2007).

[29]F. Iucolano, F. Roccaforte, F. Giannazzo, and V. Raineri, Appl. Phys. Lett. **90**, 092119 (2007).

[30]T.-H. Yang, H. Fu, H. Chen, X. Huang, J. Montes, I. Baranowski, K. Fu, and Y. Zhao, J. Semicond. **40**, 012801 (2019).

[31]J. H. Werner and H. H. Güttler, J. Appl. Phys. **69**, 1522 (1991).

[32]B. P. Modi and J. M. Dhimmar, 2012 1st International Conference on Emerging Technology Trends in Electronics, Communication & Networking (2012).

[33]Y. Son and R. L. Peterson, Semicond. Sci. Technol. **32**, 12LT02 (2017).

[34]P. P. Sundaram, F. Alema, A. Osinsky, and S. J. Koester, J. Vac. Sci. Technol. A **40**, 043211 (2022).

[35]H. Iwano, S. Zaima, and Y. Yasuda, J. Vacuum Sci. Technol. B Microelectron. Nanometer Structures Process. Meas. Phenom. **16**, 2551 (1998).

[36]D. Yu, C. Wang, B. L. Wehrenberg, and P. Guyot-Sionnest, Phys. Rev. Lett. **92**, 216802 (2004).

[37]P. Mark and W. Helfrich, J. Appl. Phys. **33**, 205 (1962).

[38]J. A. Röhr, D. Moia, S. A. Haque, T. Kirchartz, and J. Nelson, J. Phys. Condens. Matter **30**, 105901 (2018).

[39]M. P. Houng, Y. H. Wang, and W. J. Chang, J. Appl. Phys. **86**, 1488 (1999).

[40]Z. H. Liu, G. I. Ng, S. Arulkumaran, Y. K. T. Maung, and H. Zhou, Appl. Phys. Lett. **98**, 163501 (2011).

[41]W. J. Ha, S. Chhajed, S. J. Oh, S. Hwang, J. K. Kim, J.-H. Lee, and K.-S. Kim, Appl. Phys. Lett. **100**, 132104 (2012).

[42]J. Acharya, J. Wilt, B. Liu, and J. Wu, ACS Appl. Mater. Interfaces. **10**, 3112 (2018).

[43]K. Fu, H. Fu, X. Huang, T. Yang, C. Cheng, P. Peri, H. Chen, J. Montes, C. Yang, J. Zhou, X. Deng, X. Qi, D. Smith, S. Goodnick, and Y. Zhao, IEEE J. Electron Devices Soc. **8**, (2020).

[44]K. Sakowski, L. Marcinkowski, S. Krukowski, S. Grzanka, and E. Litwin-Staszewska, J. of Appl. Phys. **111**, 123115 (2012).

FIGURE CAPTIONS

Figure 1. (a) Schematic of fabricated vertical β-$(Al_xGa_{1-x})_2O_3$ (x = 0.21) SBD. (b) XRD spectrum of (020) peaks of β-Ga_2O_3 and β-$(Al_xGa_{1-x})_2O_3$. (c) 3D AFM data of the epilayer. (d) Top view of the epilayer by AFM.

Figure 2. (a) Forward current density and specific R_{ON} as a function of voltage for the vertical β-$(Al_xGa_{1-x})_2O_3$ SBD. (b) Forward current density versus voltage for the vertical β-$(Al_xGa_{1-x})_2O_3$ SBD on a semi-log scale. (c) *C-V* and $1/C^2$-*V* plots and (d) temperature-dependent *J-V* curves of the vertical β-$(Al_xGa_{1-x})_2O_3$ SBD.

Figure 3. (a) Effective Schottky barrier height (φ_{eff}) and ideality factor (n) as a function of temperature for the vertical β-$(Al_xGa_{1-x})_2O_3$ SBD. (b) n versus φ_{eff}, (c) φ_{eff} versus 1000/T, and (d) $(\frac{1}{n} - 1)$ versus 1000/T the vertical β-$(Al_xGa_{1-x})_2O_3$ SBD.

Figure 4. (a) Temperature-dependent reveres *J-V* characteristics of the vertical β-$(Al_xGa_{1-x})_2O_3$ SBD. (b) *J* versus 1000/*T* at different voltages for the vertical β-$(Al_xGa_{1-x})_2O_3$ SBD. (c) Potential leakage mechanisms in SBDs.

Figure 5. (a) Experimental and theoretical data of $\ln\left(\frac{J}{E}\right)$ versus $\sqrt{E}$ for the vertical β-$(Al_xGa_{1-x})_2O_3$ SBD. (b) The intercept $b(T)$ and the slope $m(T)$ of the curves in (a) are shown as a function of temperature. (c) Experimental and theoretical data of $\ln J$ versus $1/E$ at different temperatures.